J Mol Model (2015) 21: 19
DOI 10.1007/s00894-015-2574-8

ORIGINAL PAPER

Direct and solvent-assisted keto–enol tautomerism and hydrogen-bonding interactions in 4-(*m*-chlorobenzylamino)-3-phenyl-4,5-dihydro-1*H*-1,2,4-triazol-5-one: a quantum-chemical study

N. Burcu Arslan · Namık Özdemir

Received: 30 September 2014 / Accepted: 4 January 2015 / Published online: 25 January 2015

Abstract The tautomeric equilibrium of the title triazole compound was computationally analyzed at the B3LYP/6-311++G(d,p) and MP2/6-311++G(d,p) levels of theory. The solvent effect was considered for three solvents (chloroform, methanol, and water). Two distinct mechanisms were applied: a direct intramolecular transfer using the polarizable continuum model (PCM) and a solvent-assisted mechanism. The calculations indicated that the keto form is more stable in all cases. It was found that the barrier heights for the tautomerization reaction are very high, indicating a relatively disfavored process. Although the barrier heights for solvent-assisted reactions are significantly lower than those for the unassisted tautomerization reaction, implying the importance of the superior catalytic effect of the solvents, monosolvation was not found to be sufficient for the reaction to occur. Finally, the two intermolecular hydrogen-bonding interactions in the crystal structure were investigated in the gas phase; according to the calculated energies and structural parameters, the order of stability is N3–H3···O1>N1–H1···O1.

Keywords 1,2,4-Triazole · DFT · MP2 · Keto–enol tautomerism · Solvent effect · Hydrogen bonding

N. B. Arslan
Department of Computer Education and Instructional Technology, Faculty of Education, Giresun University, 28100 Giresun, Turkey

N. Özdemir (✉)
Department of Physics, Faculty of Arts and Sciences, Ondokuz Mayıs University, 55139 Samsun, Turkey
e-mail: namiko@omu.edu.tr

Introduction

Tautomeric equilibria play fundamental roles in many organic and biochemical reactions, in structural assignments, and in the biochemical activities of amino acids, sugars, and nucleic acids [1–5]. Tautomerism is an interconversion between isomeric forms that involves proton transportation and a double-bond (π-electron) shift. Keto–enol, thione–thiol, enamine–imine, acinitro–nitro, nitroso–oxime, and amide–iminole transformations can be considered the most common types of tautomerism [6]. Among these, keto–enol tautomerism plays a crucial role in compounds with a carbonyl group. Investigations of the tautomeric equilibria associated with carbonyl compounds are very important for rationalizing their biological activities and for understanding the biochemical processes in which they take part [7–17].

One of the most important interactions that influences the arrangement of molecules in crystals is the hydrogen bond [18, 19]. Hydrogen bonds are commonly encountered in both chemistry and biochemistry [19–21]. Perhaps the most important application of hydrogen-bonding interactions is in the interactions that determine the shapes of proteins and the genetic code information in DNA and RNA [22–24].

One important class of compounds that exhibit keto–enol tautomerism are the carbonyl derivatives of 1,2,4-triazole. 1,2,4-Triazoles are well known to have various types of biological activities, such as anti-inflammatory [25, 26], antiviral [27], analgesic [28], antimicrobial [29], anticonvulsant [30], anticancer [31], antioxidant [32], antitumoral [33], and antidepressant [34] activities. It has also been reported that some coordination complexes with 1,2,4-triazole as a ligand possess interesting structures and magnetic properties [35–38]. To carry out structure–activity or molecular docking studies of such

systems, knowledge of the relative stabilities of the keto and enol tautomers involved is required, since the interactions of compounds with bacterial enzymes can change in the presence of a hydroxyl or a carbonyl group [7]. Moreover, knowing how the tautomerization energies change in different solvents affords insight into the influence of solvents on molecular stability and reactivity.

In the work reported in this paper, we investigated the mechanism of keto–enol tautomerism and intermolecular H-bonding interactions for the title compound using density functional theory (DFT). Single-point energy calculations were also performed at the MP2 level for the tautomeric mechanism. The effect of solvent on the tautomerism was studied by applying the polarizable continuum model (PCM) and directly involving the solvent molecules.

Computational details

The structures at the local minimum or the transition state (TS) were optimized using the Berny algorithm [39] and default cutoffs. The minimum-energy or transition-state nature of the stationary points was verified from frequency analysis. The stable structures only exhibited positive frequencies, whereas the TSs each possessed one imaginary frequency. All calculations were performed via the GaussView molecular visualization program [40] and the Gaussian 03W package [41]. The three-parameter hybrid density functional (B3LYP) [42, 43] and the 6-311++G(d,p) basis set [44, 45] were selected for the calculations. We also performed single-point energy calculations at the MP2 (second-order Møller–Plesset perturbation theory) level of theory [46] with the 6-311++G(d,p) basis set for B3LYP/6-311++G(d,p) geometries. DFT and MP2 levels of theory have been successfully used to study similar systems recently, and have been shown to give accurate normal-mode frequencies, barrier heights, characteristics of intra- and intermolecular H-bonds, and geometries [14, 15]. To connect the transition states to their respective minima, the reaction pathway was followed in both the forward and reverse directions from each TS using the intrinsic reaction coordinate (IRC) procedure [47, 48]. The binding energies of the intermolecular H-bonding interactions were obtained using the supermolecule approach [49, 50], and were corrected for basis set superposition error (BSSE) via the standard counterpoise method [51]. Solvent effects in chloroform, methanol, and water were calculated by means of the PCM method [52–55] at the B3LYP/6-311++G(d,p) level. The thermodynamic parameters were obtained from the frequency analyses of the optimized structures, and were computed using the thermodynamic equations and $\Delta G=\Delta H - T\Delta S$ [56, 57].

Results and discussion

Theoretical structures

We determined the solid-state structure of the compound (Fig. 1a) in a previous work [58]. The molecular structure was optimized by the density functional theory (DFT) method with the 6-311++G(d,p) basis set (Fig. 1b). Some of the experimental and theoretical geometric parameters calculated in the gas phase and in solution are collected in Table 1.

As can be seen in Table 1, the optimized structures closely resemble the experimental one. X-ray study reveals that the triazole ring makes dihedral angles of 2.95(14)° and 16.43 (12)° with the planes of the chlorophenyl and benzene rings, respectively. These angles were calculated as 4.13° and 23.48° in the gas phase, 2.62° and 31.72° in chloroform, 1.66° and 33.99° in methanol, and 1.44° and 34.31° in water, respectively. In addition, the dihedral angle between the chlorophenyl and benzene rings was found to be 19.29(11)° experimentally, while it was determined theoretically as 19.97°, 31.34°, 33.57°, and 33.86° in the gas phase, chloroform, methanol, and in water. When the optimized and experimental structures of the molecule were compared by overlaying them using a least-squares algorithm that minimizes the distances between the corresponding non-hydrogen atoms, as shown in Fig. 1c, the resulting RMSEs were 0.179, 0.151, 0.169, and 0.172 Å, respectively, in the gas phase, chloroform, methanol, and in water (Fig. 1c). So, these results show that the level of theory adequately describes the experimental geometry and can be used to study the reaction mechanism of the keto–enol tautomerism displayed by the title compound.

In order to prove that the structure presented in this work is the global minimum, a preliminary search of low-energy structures was performed using the B3LYP/6-311++G(d,p) computations as a one-dimensional scan by varying the φ_1(N2–N1–C7–C6) and φ_2(N2–C9–C10–C15) torsion angles from −180° to 180° in steps of 10°. Molecular energy profiles with respect to rotations around the N1–C7 and C9–C10 bonds are presented in Fig. 2. It can be seen from the figure that the lowest-energy domain is located at −170° for φ_1(N2–N1–C7–C6) and at 160° for φ_2(N2–C9–C10–C15), which are in agreement with the optimized values of −171° and 157°.

Direct keto–enol tautomerism

As can be seen in Fig. 3, there are two possible tautomeric forms for the compound: keto and enol; the former has an exocyclic C8=O1 double bond and the latter has an endocyclic C8=N3 double bond. The geometric parameters for the keto and enol and the corresponding TS geometries of the compound are also collected in Table 1, while their energetic parameters are given in Table 2. The imaginary frequency at the transition state was found to be 1915*i* cm^{-1} in

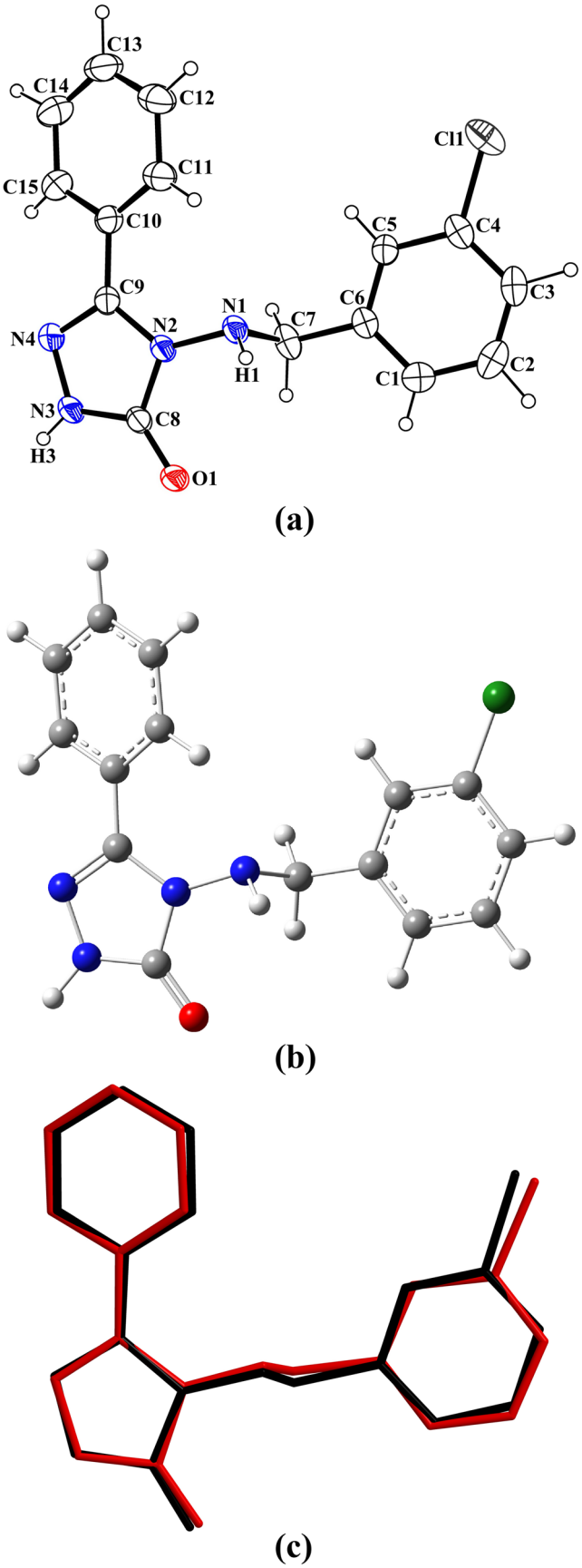

Fig. 1 **a** Experimental structure of the title compound, along with the atom-numbering scheme used in this work [42]. **b** Theoretical structure of the title compound. **c** Superposition of the experimental (*black*) and calculated (*red*) structures. Hydrogen atoms are omitted for clarity

the gas phase, 1945*i* cm^{-1} in chloroform, 1958*i* cm^{-1} in methanol, and 1960*i* cm^{-1} in water.

The keto and enol tautomers can transform into each other via an intramolecular proton-transfer reaction. Because of the migration of a hydrogen atom from atom N3 to atom O1, some changes are observed in the structure. The distance between atoms O1 and H3 decreases upon the proton transfer associated with keto→TS→enol. It can be concluded that the N3–H3 bond is broken and an O1–H3 bond (0.967 Å in the gas phase and 0.968 Å in all solvent media) is formed during the intramolecular proton-transfer process in the compound. On going from the keto to the enol monomer, the N3–C8 bond length is reduced by 0.072 Å in the gas phase, 0.065 Å in chloroform, and 0.061 Å in methanol and water, while the O1–C8 distance is increased by 0.125 Å in the gas phase, 0.113 Å in chloroform, and 0.108 Å in methanol and water. This is consistent with scission of the C=O double bond and the corresponding formation of a C=N double bond. In addition, a lengthening of the N3—N4 bond and a shortening of the N2—C8 bond are observed. Among the bond angles, the C8–N2–C9, C8–N3–N4, O1–C8–N3, O1–C8–N2, and N4–C9–N2 angles contract while the C8–N2–N1, C9–N4–N3, and N3–C8–N2 angles expand. The N3···H3 and O1···H3 lengths in the TS structure were computed to be 1.340 and 1.402 Å in the gas phase, 1.338 and 1.401 Å in chloroform, and 1.336 and 1.401 Å in methanol and water, respectively.

It should be mentioned here that the molecule is soft and has low-lying vibrational modes in its vibrational spectrum related to the torsion angles φ_1(N2–N1–C7–C6) and φ_2(N2–C9–C10–C15). It has been shown that the deformation of the molecule at the transition state from the isolated state or solution or crystal can be fully explained by its softness [59].

Figure 4 shows the potential energy diagram for the keto–enol isomerization of the title compound. The energy difference between the two tautomers was calculated to be −76.15, −69.94, −66.73, and −66.33 kJ mol^{-1} in the gas phase, chloroform, methanol, and water, respectively. Single-point energy calculations provided slightly smaller values (−73.63, −68.02, −64.88, and −64.49 kJ mol^{-1}, respectively). According to the ground-state energies of the enol and keto tautomers and the tautomerization energies shown in Table 2, the calculations predict the keto form to be the most stable in the gas phase and in solution. The calculated IRC profile for the direct proton-transfer reaction is presented in Fig. 5. It is clear that the investigated proton-transfer reactions involve concerted atomic movement. This means that the proton transfers happen in a single step without any intermediate.

Table 1 Experimental and optimized structural parameters of the keto–enol tautomers and transition state of the title compound

Parameters	X-ray	Gas phase			Chloroform (ε=4.90)			Methanol (ε=32.63)			Water (ε=78.39)		
		Keto	TS	Enol	Keto	TS	Enol	Keto	TS	Enol	Keto	TS	Enol
Bond lengths (Å)													
O1—C8	1.2381(19)	1.218	1.285	1.343	1.224	1.288	1.337	1.226	1.289	1.334	1.226	1.289	1.334
O1—H3	–	–	–	0.967	–	–	0.968	–	–	0.968	–	–	0.968
N1—N2	1.4054(17)	1.398	1.400	1.401	1.397	1.399	1.401	1.397	1.399	1.400	1.397	1.399	1.400
N2—C8	1.380(2)	1.405	1.359	1.368	1.403	1.358	1.368	1.402	1.358	1.369	1.402	1.358	1.369
N2—C9	1.381(2)	1.391	1.421	1.395	1.389	1.417	1.390	1.388	1.415	1.388	1.388	1.414	1.388
N3—C8	1.332(2)	1.368	1.312	1.296	1.365	1.312	1.300	1.363	1.312	1.302	1.363	1.312	1.302
N3—N4	1.374(2)	1.375	1.377	1.390	1.376	1.380	1.393	1.376	1.382	1.394	1.376	1.382	1.395
N3—H3	0.79(2)	1.006	–	–	1.008	–	–	1.008	–	–	1.008	–	–
N4—C9	1.299(2)	1.305	1.312	1.311	1.305	1.313	1.312	1.306	1.314	1.312	1.306	1.313	1.312
Bond angles (°)													
C8–N2–C9	108.47(12)	109.04	104.36	103.98	108.83	104.40	104.33	108.76	104.42	104.47	108.75	104.42	104.49
C8–N2–N1	124.60(12)	122.84	127.58	127.37	124.04	128.44	127.77	124.38	128.81	127.93	124.42	128.89	127.95
C9–N2–N1	126.84(13)	128.06	127.79	128.43	126.99	126.90	127.66	126.71	126.50	127.38	126.67	126.41	127.34
C8–N3–N4	113.12(15)	113.87	110.99	106.32	113.73	110.91	106.38	113.67	110.88	106.39	113.66	110.88	106.39
C8–N3–H3	129.1(15)	125.89	–	–	126.02	–	–	126.07	–	–	126.07	–	–
C8–O1–H3	–	–	–	107.28	–	–	108.60	–	–	109.04	–	–	109.09
N4–N3–H3	117.7(15)	120.13	–	–	120.15	–	–	120.18	–	–	120.18	–	–
C9–N4–N3	105.32(13)	105.45	105.42	108.82	105.32	105.19	108.62	105.28	105.08	108.57	105.28	105.06	108.56
O1–C8–N3	129.87(16)	131.33	110.96	128.04	130.83	110.55	128.52	130.67	110.40	128.67	130.64	110.38	128.69
O1–C8–N2	126.78(13)	127.10	140.15	119.92	127.28	140.52	119.79	127.31	140.67	119.77	127.32	140.70	119.77
N3–C8–N2	103.34(13)	101.57	108.89	112.03	101.89	108.93	111.69	102.02	108.92	111.55	102.03	108.92	111.54
N4–C9–N2	109.72(14)	110.08	110.33	108.84	110.23	110.57	108.97	110.27	110.69	109.02	110.28	110.71	109.02

ε dielectric constant

The forward reaction barrier—encountered during proton transfer from the keto to the enol form of the compound—was computed as 262.24, 264.01, 264.22, and 264.21 kJ mol^{-1} in the gas phase, in chloroform, in methanol, and in water, respectively. These values show that a great deal of energy is required for the forward proton transfer to occur. For the

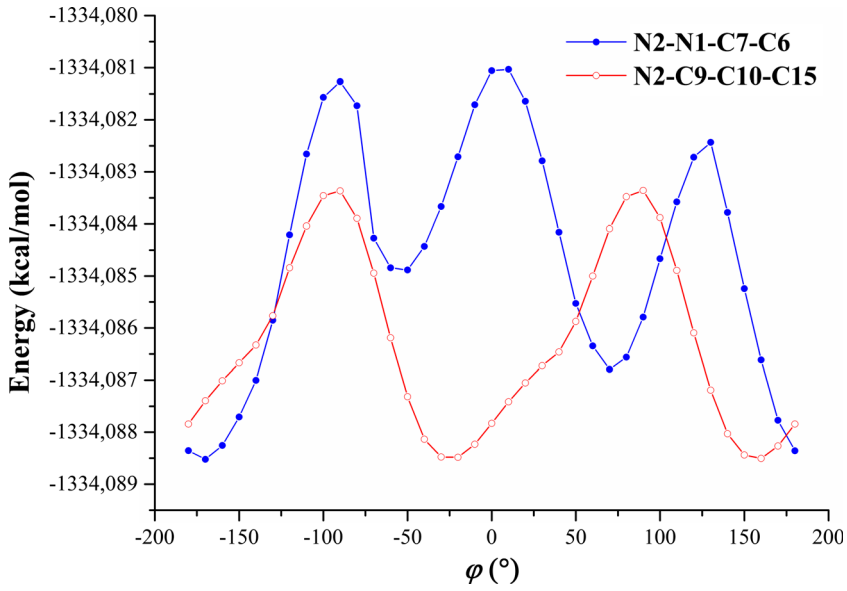

Fig. 2 Molecular energy profiles of the title compound for selected degrees of torsional freedom

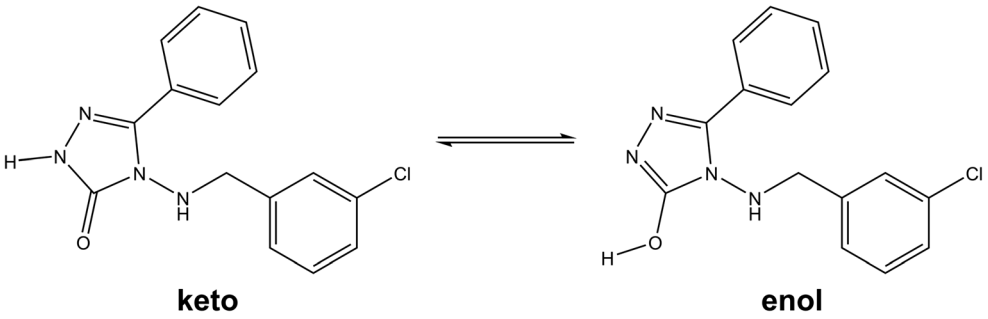

Fig. 3 Schematic representation of possible tautomers of the title compound

reverse reaction, the barrier height was calculated as 186.09, 194.07, 197.49, and 197.88 kJ mol^{-1} in the gas phase, in chloroform, in methanol, and in water, respectively. The MP2 results predict larger barrier heights: 327.49, 329.48, 329.43, and 329.36 kJ mol^{-1} for the forward reaction and 253.86, 261.46, 264.55, and 264.88 kJ mol^{-1} for the reverse reaction, respectively. Consequently, neither the forward nor the reverse reaction appears to happen spontaneously. The standard enthalpy and free-energy changes associated with the keto ↔ enol tautomerism are also tabulated in Table 2. According to the calculated thermodynamic parameters, the single proton-transfer reaction in both directions is strongly endothermic, with large positive standard enthalpy and free-energy changes in all phases. As a result, we can deduce that the single proton-transfer reaction between the keto and enol tautomers is not a favored process.

Solvent-assisted keto–enol tautomerism

We also investigated the keto ↔ enol tautomerism in the presence of a single solvent molecule. In this case, the imaginary frequency at the transition state was found to be 235*i* cm^{-1} for chloroform, 1142*i* cm^{-1} for methanol, and 1499*i* cm^{-1} for water. The structural parameters shown in Fig. 6 display significant geometric changes as the tautomerism proceeds. Complexation with a single solvent molecule has a significant effect on the geometries of the keto and enol moieties, and mainly influences the geometric parameters in the vicinity of the intermolecular hydrogen-bonding region.

The energies of the keto and enol forms complexed with the solvent molecules, energy differences, activation energies, and standard enthalpy and free-energy changes are given in Table 3. The energy separation between the two tautomers was found to be −68.56, −54.90, and −56.59 kJ mol^{-1} for B3LYP, and −89.99, −72.15, and −71.60 kJ mol^{-1} for MP2, in chloroform, methanol, and water, respectively. The keto form is therefore more stable than the enol form. The IRC profile for the solvent-assisted proton-transfer reaction is presented in Fig. 7. It can be seen from the figure that the proton-transfer reactions occur in a single step without any intermediates.

The relative energies of the TS with respect to the keto tautomer were obtained as 219.59, 93.83, and 100.93 kJ mol^{-1}, while the reverse reaction barriers were calculated as 151.03, 38.92, and 44.34 kJ mol^{-1} in chloroform, methanol, and water, respectively. The MP2 barrier heights were found to be higher than those of B3LYP: 236.21, 151.31, and 156.57 kJ mol^{-1} for the forward reaction and 146.22, 79.16, and 89.96 kJ mol^{-1} in chloroform, methanol, and water, respectively. Compared with the direct proton-transfer process in the presence of bulk solvent, it is clear that the intervention of a solvent molecule considerably reduces the energy barrier and the enthalpy and free-energy changes. However, the large positive standard enthalpy and free-energy changes as well as the tautomeric energy barrier reveal that a substantial amount of energy is still necessary for either the forward or the reverse proton transfer to occur in the presence of one solvent molecule, indicating a process that is disfavored or not spontaneous.

Table 2 Energies of the keto and enol forms of the title 1,2,4-triazole compound in hartrees, and energy differences, activation energies, and thermodynamic parameters in kJ mol^{-1}

	Keto	Enol	ΔE	E_a(f)	E_a(r)	ΔH_{298}(f)	ΔG_{298}(f)	$T\Delta S_{298}$(f)	ΔH_{298}(r)	ΔG_{298}(r)	$T\Delta S_{298}$(r)
Gas phase	−1334.08852320	−1334.05952069	−76.15	262.24	186.09	246.02	245.24	0.78	171.69	171.41	0.28
Chloroform	−1334.09869408	−1334.07205559	−69.94	264.01	194.07	248.01	249.10	−1.09	179.62	182.07	−2.45
Methanol	−1334.10252840	−1334.07711225	−66.73	264.22	197.49	248.10	246.80	1.29	182.79	181.51	1.28
Water	−1334.10296163	−1334.07769730	−66.33	264.21	197.88	248.03	245.34	2.69	183.10	180.47	2.63

$\Delta E = E_{keto} - E_{enol}$, E_a(f) = forward activation energy, E_a(r) = reverse activation energy

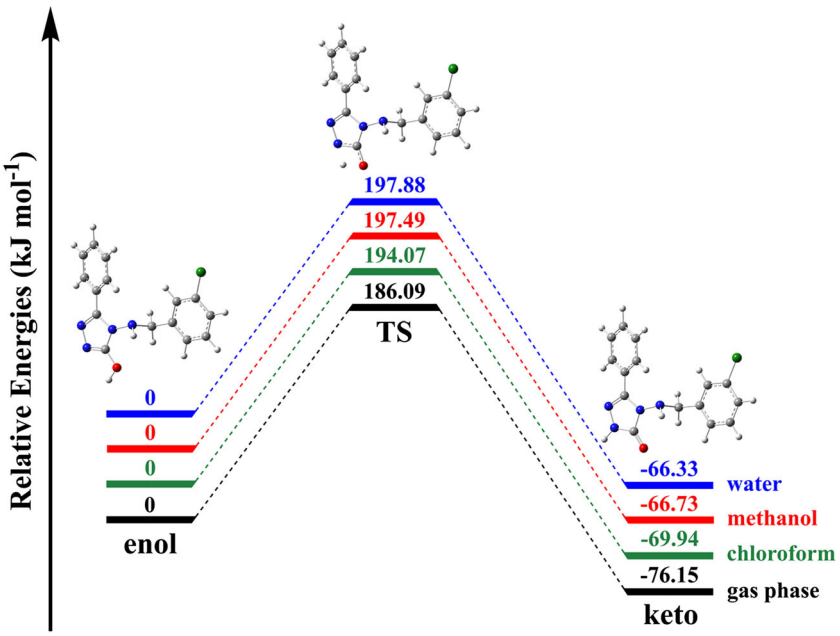

Fig. 4 Potential energy diagram for the direct keto–enol tautomerism of the title compound in the gas phase and in various solvents

Intermolecular hydrogen-bonding interactions

The geometric and energetic properties of the intermolecular hydrogen-bonding interactions of the compound were investigated at the same level of theory in the gas phase, and the results are collected in Table 4, together with the corresponding experimental values.

In the crystal structure of the compound, two intermolecular interactions are observed, N1–H1···O1 and N3–H3···O1, which form centrosymmetric dimers characterized as $R_2^2(10)$ and $R_2^2(8)$ motifs [60], respectively. It is apparent from the table that the computed hydrogen bond lengths are 1.948 and 1.843 Å for the N1–H1···O1 and N3–H3···O1 interactions, respectively, which are shorter than those observed experimentally. Because of the hydrogen-bonding interactions, the bond lengths N1–H1 and N3–H3 were calculated to be slightly longer, by 0.174 and 0.237 Å, respectively, than those in the free keto tautomer. Although the collinear bond angle of the N1–H1···O1 interaction was found to be more linear than that of the N3–H3···O1 interaction (177° versus 163°), the remaining geometrical parameters of the two interactions are consistent with the experimental values, which demonstrate that the N3–H3···O1 interaction is stronger than the N1–H1···O1 interaction.

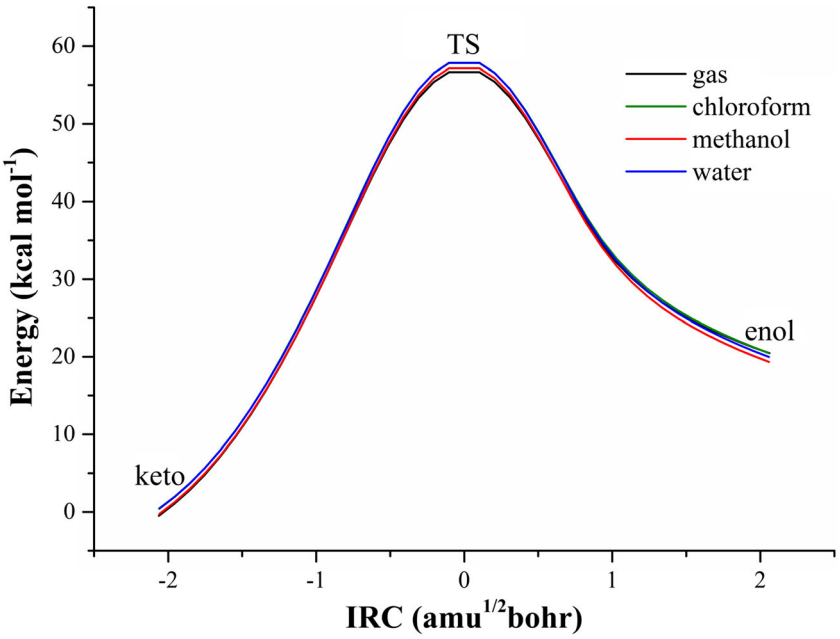

Fig. 5 Profiles of the relative total energy versus the intrinsic reaction coordinate (IRC) for the direct keto–enol tautomerism of the title compound in the gas phase and in various solvents, as calculated at the B3LYP/6-311++G(d,p) level of theory

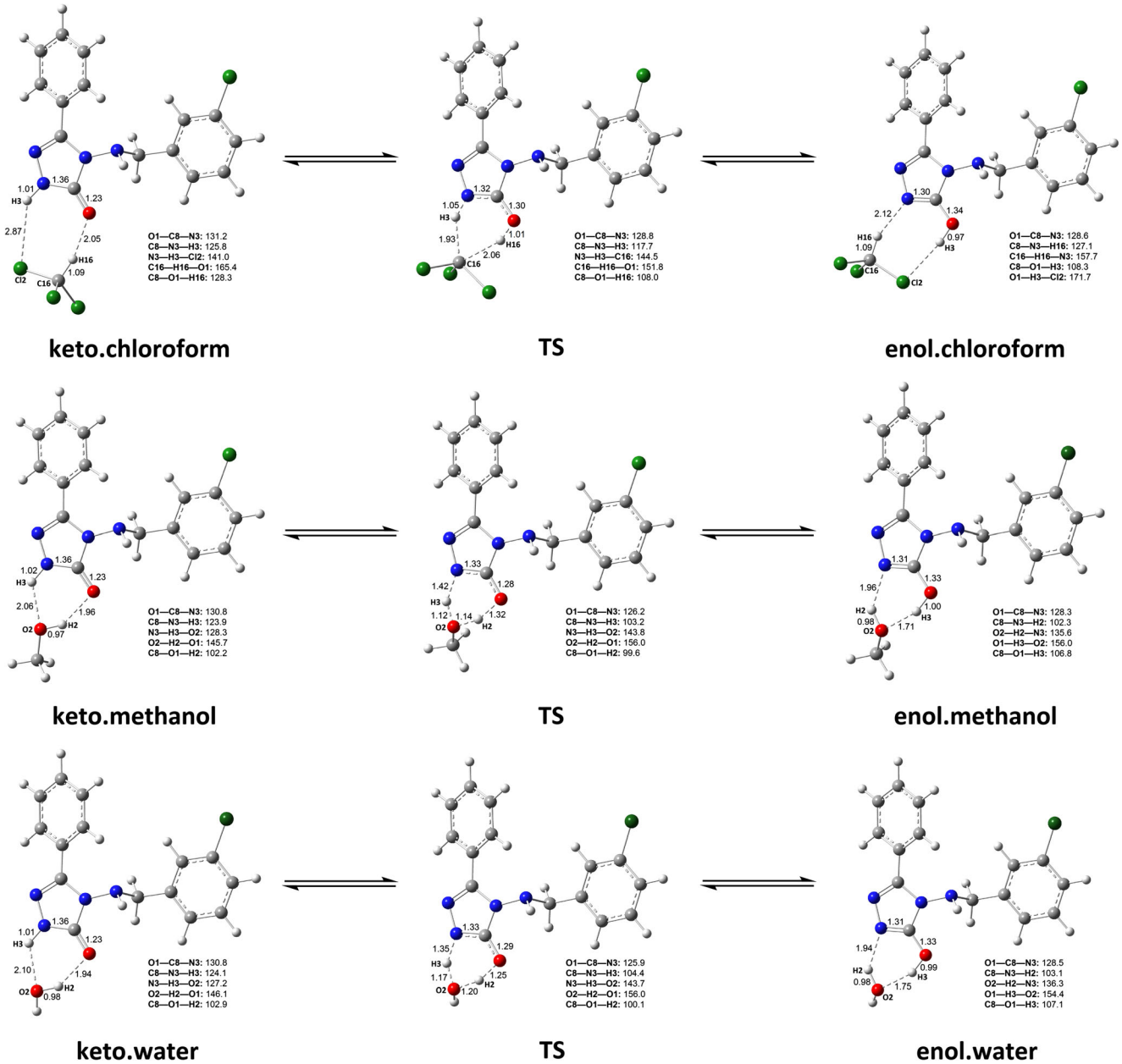

Fig. 6 Mechanism of the solvent-assisted tautomerization between keto and enol complexes by double proton transfer. Distances are in Å and angles are in degrees

The computational results show that the cyclic dimer constructed via two N3–H3···O1 interactions is more thermodynamically stable than the other dimer formed via two N1–H1···O1 interactions, the difference between their

Table 3 Energies of the keto and enol tautomers complexed with the solvent molecules in hartrees, and energy differences, activation energies, and thermodynamic parameters in kJ mol^{-1}

	Keto	Enol	ΔE	E_a(f)	E_a(r)	ΔH_{298}(f)	ΔG_{298}(f)	$T\Delta S_{298}$(f)	ΔH_{298}(r)	ΔG_{298}(r)	$T\Delta S_{298}$(r)
Chloroform	−2753.47729362	−2753.45117928	−68.56	219.59	151.03	208.83	221.62	−12.79	142.09	148.50	−6.41
Methanol	−1449.86841509	−1449.84750429	−54.90	93.83	38.92	75.30	86.07	−10.76	21.69	28.96	−7.27
Water	−1410.56216730	−1410.54061441	−56.59	100.93	44.34	80.97	91.52	−10.55	25.61	32.82	−7.21

$\Delta E = E_{keto.solvent} - E_{enol.solvent}$, E_a(f)=forward activation energy, E_a(r) = reverse activation energy

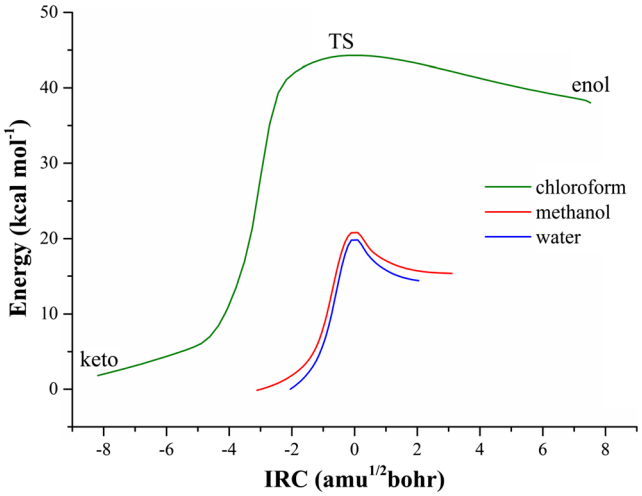

Fig. 7 Profiles of the relative total energy versus the intrinsic reaction coordinate (IRC) for the solvent-assisted keto–enol tautomerism of the title compound, as calculated at the B3LYP/6-311++G(d,p) level of theory

total energies being −19.08 kJ mol^{-1}. As can be seen from Table 4, the BSSE-corrected binding energies were found to be −19.00 and −30.96 kJ mol^{-1} for the N1–H1···O1 and N3–H3···O1 interactions, respectively.

The energies of the intermolecular H-bonds, in kcal mol^{-1}, were also evaluated using the empirical Iogansen relationship [61]

$$E = 0.33\sqrt{\Delta\nu - 40},$$

where $\Delta\nu$ (cm^{-1}) is the magnitude of the redshift (relative to the free molecule) of the stretching mode of the H-bonded groups involved in the H-bonding. According to the formula, the intermolecular N1–H1···O1 and N3–H3···O1 interactions have energies of 3.33 and 6.07 kcal mol^{-1}, respectively. Hence, the N3–H3···O1 hydrogen bond is stronger than the N1–H1···O1 bond.

Table 4 Intermolecular H-bond geometries and interaction energies (kJ mol^{-1}) in the gas phase

Parameters	N1–H1···O1		N3–H3···O1	
	Experimental	Theoretical	Experimental	Theoretical
D–H (Å)	0.850(19)	1.024	0.79(2)	1.027
H···A (Å)	2.15(2)	1.948	2.06(2)	1.843
D···A (Å)	2.981(2)	2.971	2.832(2)	2.840
D–H···A (°)	164(2)	177	167(3)	163
E	–	−21.93	–	−32.51
E_{CP}	–	−19.00	–	−30.96
E^{def}	–	1.77	–	2.81
E^{opt}	–	−17.23	–	−28.15

E = uncorrected binding energy, E_{CP}=BSSE corrected binding energy, E^{def} = deformation energy,

E^{opt} =BSSE-corrected total interaction energy

Table 5 Calculated Mulliken charges (e) on key atoms involved in the interactions in the gas phase

Atom	Keto	Interaction		ΔQ
		N1–H1···O1	N3–H3···O1	
O1	−0.392	−0.379	−0.419	0.013/−0.027
N1	−0.04	−0.220	–	−0.18
N3	−0.183	–	−0.365	−0.182
H1	0.273	0.403	–	0.13
H3	0.314	–	0.450	0.136

The computed Mulliken charges on the donor, hydrogen, and acceptor atoms in the two intermolecular interactions are given in Table 5; ΔQ is the change in the charge on the atoms because of the intermolecular hydrogen-bonding interactions. All of the atoms involved in the hydrogen bonding present a change in charge, and the variations in the charges on the donor, acceptor, and hydrogen atoms are not the same for the two H-bonds. In the N1–H1···O1 interaction, the nitrogen atom is more negative and the hydrogen atom is more positive, while the oxygen atom is less negative. In the N3–H3···O1 interaction, the nitrogen and oxygen atoms are more negative, while the hydrogen atom is more positive. The net charges ($\Delta Q_{donor}+\Delta Q_{hydrogen}+\Delta Q_{acceptor}$), which are −0.037$e$ for the N1–H1···O1 hydrogen bond and −0.073 for the N3–H3···O1 hydrogen bond, indicate that the neighboring atoms are also included in the charge transfer.

Conclusions

In this paper we have reported the results we obtained at the B3LYP/6-311++G(d,p) level of theory for the structural parameters, the direct and solvent-assisted keto–enol tautomerism, and the intermolecular hydrogen-bonding interactions in the title 1,2,4-triazole compound. When exploring the tautomeric mechanism, additional single-point energy calculations were also carried out at the MP2/6-311++G(d,p) level. The calculated values for the structural parameters of the molecule were found to be in good accord with the corresponding experimental values. It was calculated that the keto form is the predominant tautomer in all phases. Very high barrier heights were found for the keto ↔ enol tautomerization process, so this tautomerization does not occur spontaneously in the gas phase or in solution. When a single molecule of solvent participated in the proton-transfer reaction, it was found that the barrier heights decreased significantly. Even though the

calculated values still suggested that the tautomerization was unfavorable, it was clear that including more solvent molecules in the proton-transfer reaction not only lowers the positive standard free energy but also greatly reduces the activation energy. According to the energy values obtained for the hydrogen-bonding interactions, the N3–H3···O1 intermolecular hydrogen bond contributes more to the stability of the crystal structure than the N1–H1···O1 hydrogen bond does.

Acknowledgments We would like to thank the reviewers for their helpful comments and suggestions to improve the manuscript.

References

1. Cucinotta CS, Ruini A, Catellani A, Stirling A (2006) Ab initio molecular dynamics study of the keto-enol tautomerism of acetone in solution. ChemPhysChem 7(6):1229–1234
2. Brovarets' OO, Hovorun DM (2013) Prototropic tautomerism and basic molecular principles of hypoxanthine mutagenicity: an exhaustive quantum-chemical analysis. J Biomol Struct Dyn 31(8):913–936
3. Samijlenko SP, Yurenko YP, Stepanyugin V, Hovorun DM (2011) Tautomeric equilibrium of uracil and thymine in model protein–nucleic acid contacts. Spectroscopic and quantum chemical approach. J Phys Chem B 114(3):1454–1461
4. Brovarets' OO, Hovorun DM (2010) How stable are the mutagenic tautomers of DNA bases? Biopolym Cell 26(1):72–76
5. Brovarets' OO, Hovorun DM (2010) Stability of mutagenic tautomers of uracil and its halogen derivatives: the results of quantum-mechanical investigation. Biopolym Cell 26(4):295–298
6. Smith MB, March J (2001) March's advanced organic chemistry. Wiley, New York
7. Pitucha M, Karczmarzyk Z, Wysocki W, Kaczor AA, Matosiuk D (2011) Experimental and theoretical investigations on the keto–enol tautomerism of 4-substituted 3-[1-methylpyrrol-2-yl)methyl]-4,5-dihydro-1*H*-1,2,4-triazol-5-one derivatives. J Mol Struct 994(1–3): 313–320
8. Matosiuk D, Fidecka S, Antkiewicz-Michaluk L, Lipkowski J, Dybala I, Koziol AE (2002) Synthesis and pharmacological activity of new carbonyl derivatives of 1-aryl-2-iminoimidazolidine. Part 2. Synthesis and pharmacological activity of 1,6-diaryl-5,7(1*H*)dioxo-2,3-dihydroimidazo[1,2-*a*]-[1,3,5]triazines. Eur J Med Chem 37(9): 761–772
9. Matosiuk D, Fidecka S, Antkiewicz-Michaluk L, Dybala I, Koziol AE (2002) Synthesis and pharmacological activity of new carbonyl derivatives of 1-aryl-2-iminoimidazolidine. Part 3. Synthesis and pharmacological activity of 1-aryl-5,6(1*H*)dioxo-2,3-dihydroimidazo[1,2-*a*]imidazoles. Eur J Med Chem 37(10):845–853
10. Sztanke K, Fidecka S, Kedzierska E, Karczmarzyk Z, Pihlaja K, Matosiuk D (2005) Antinociceptive activity of new imidazolidine carbonyl derivatives. Part 4. Synthesis and pharmacological activity of 8-aryl-3,4-dioxo-2*H*,8*H*-6,7-dihydroimidazo[2,1-*c*][1,2,4]triazines. Eur J Med Chem 40(2):127–134
11. Temperini C, Cecchi A, Scozzafava A, Supuran CT (2009) Carbonic anhydrase inhibitors. Comparison of chlorthalidone and indapamide X-ray crystal structures in adducts with isozyme II: when three water molecules and the keto–enol tautomerism make the difference. J Med Chem 52(2):322–328
12. Brovarets' OO, Hovorun DM (2014) Can tautomerization of the A·T Watson–Crick base pair via double proton transfer provoke point mutations during DNA replication? A comprehensive QM and QTAIM analysis. J Biomol Struct Dyn 32(1):127–154
13. Brovarets' OO, Hovorun DM (2014) Why the tautomerization of the G·C Watson–Crick base pair via the DPT does not cause point mutations during DNA replication? QM and QTAIM comprehensive analysis. J Biomol Struct Dyn 32(9):1474–1499
14. Brovarets' OO, Hovorun DM (2015) The physicochemical essence of the purine·pyrimidine transition mismatches with Watson–Crick geometry in DNA: A·C* versa A*·C. A QM and QTAIM atomistic understanding. J Biomol Struct Dyn 33(1):28–55. doi:10.1080/07391102.2013.852133
15. Brovarets' OO, Hovorun DM (2014) The nature of the transition mismatches with Watson–Crick architecture: the G*·T or G·T* DNA base mispair or both? A QM/QTAIM perspective for the biological problem. J Biomol Struct Dyn 23:1–21. doi:10.1080/07391102.2014.924879
16. Kosenkov D, Kholod Y, Gorb L, Shishkin O, Hovorun DM, Mons M, Leszczynski J (2009) Ab initio kinetic simulation of gas-phase experiments: tautomerization of cytosine and guanine. J Phys Chem B 113(17):6140–6150
17. Furmanchuk A, Isayev O, Shishkin OV, Hovorun DM, Leszczynski J (2011) Novel view on the mechanism of water-assisted proton transfer in the DNA bases: bulk water hydration. Phys Chem Chem Phys 13(10):4311–4317
18. Jeffrey GA, Saenger W (1991) Hydrogen bonding in biological structures. Springer, Berlin
19. Jeffrey GA (1997) An introduction to hydrogen bonding. Oxford University Press, New York
20. Desiraju GR, Steiner T (1999) The weak hydrogen bond in structural chemistry and biology. Oxford University Press, Oxford
21. Yurenko YP, Zhurakivsky RO, Samijlenko SP, Ghomi M, Hovorun DM (2007) The whole of intramolecular H-bonding in the isolated DNA nucleoside thymidine. AIM electron density topological study. Chem Phys Lett 447(1–3):140–146
22. Sahu PK, Chaudhari A, Lee S-L (2004) Theoretical investigation for the hydrogen bond interaction in THF–water complex. Chem Phys Letters 386(4–6):351–355
23. Ponomareva AG, Yurenkoa YP, Zhurakivsky RO, van Mourik T, Hovorun DM (2012) Complete conformational space of the potential HIV-1 reverse transcriptase inhibitors d4U and d4C. A quantum chemical study. Phys Chem Chem Phys 14(19):6787–6795
24. Ponomareva AG, Yurenkoa YP, Zhurakivsky RO, van Mourik T, Hovorun DM (2012) Structural and energetic properties of the potential HIV-1 reverse transcriptase inhibitors d4A and d4G: a comprehensive theoretical investigation. J Biomol Struct Dyn 32(5):730–740
25. Unangst PC, Shrum GP, Connor DT, Dyer RD, Schrier DJ (1992) Novel 1,2,4-oxadiazoles and 1,2,4-thiadiazoles as dual 5-lipoxygenase and cyclooxygenase inhibitors. J Med Chem 35(20): 3691–3698
26. Mullican MD, Wilson MW, Connor DT, Kostlan CR, Schrier DJ, Dyer RD (1993) Design of 5-(3,5-di-tert-butyl-4-hydroxyphenyl)-1, 3,4-thiadiazoles, -1,3,4-oxadiazoles, and -1,2,4-triazoles as orally-active, nonulcerogenic antiinflammatory agents. J Med Chem 36(8): 1090–1099
27. Jones DH, Slack R, Squires S, Wooldridge KRH (1965) Antiviral chemotherapy. I. The activity of pyridine and qinoline derivatives against neurovaccinia in mice. J Med Chem 8(5):676–680
28. Sughen JK, Yoloye T (1978) Medicinal applications of indole derivatives. Pharm Acta Helv 53(3–4):65–92
29. Shams El-Dine SA, Hazzaa AAB (1974) Synthesis of compounds with potential fungicidal activity. Pharmazie 29:761–763
30. Stillings MR, Welbourn AP, Walter DS (1986) Substituted 1,3,4-thiadiazoles with anticonvulsant activity. 2. Aminoalkyl derivatives. J Med Chem 29(11):2280–2284
31. Sztanke K, Tuzimski T, Rzymowska J, Pasternak K, Kandefer-Szerszeń M (2008) Synthesis, determination of the lipophilicity,

anticancer and antimicrobial properties of some fused 1,2,4-triazole derivatives. Eur J Med Chem 43(2):404–419
32. Ilango K, Valentina P (2010) Synthesis and biological activities of novel 1,2,4-triazolo-[3,4-*b*]-1,3,4-thiadiazoles. Der Pharm Chem 2(2):16–22
33. Demirbas N, Ugurluoglu D, Demirbas A (2002) Synthesis of 3-alkyl (aryl)-4-alkylidenamino-4,5-dihydro-1*H*-1,2,4-triazol-5-ones and 3-alkyl-4-alkylamino-4,5-dihydro-1*H*-1,2,4-triazol-5-ones as antitumor agents. Bioorg Med Chem 10(12):3717–3723
34. Kane JM, Dudley MW, Sorensen SM, Miller FP (1988) 2,4-Dihydro-3*H*-1,2,4-triazole-3-thiones as potential antidepressant agents. J Med Chem 31(6):1253–1258
35. Vreugdenhil W, Haasnoot JG, Reedijk J, Spek AL (1987) Ferromagnetic and antiferromagnetic spin coupling in Ni_4O_4 cubane-type clusters with 4-amino-3,5-bis(hydroxymethyl)-1,2,4-triazole as a ligand. The X-ray structure of a new dumbbell-like double cubane cluster. Inorg Chim Acta 129(2):205–216
36. Van Albada GA, De Graaff RAG, Haasnoot JG, Reedijk J (1984) Synthesis, spectroscopic characterization, and magnetic properties of unusual 3,5-dialkyl-1,2,4-triazole compounds containing N-bridging isothiocyanato ligands. X-ray structure of trinuclear bis[(μ-thiocyanato-*N*)bis(μ-3,5-diethyl-1,2,4-triazole-N^1,N^2)bis (thiocyanato-*N*)(3,5-diethyl-1,2,4-triazole-N^1)nickel(II)-*N*,N^1,$N^{1'}$] nickel(II) dihydrate. I. Inorg Chem 23(10):1404–1408
37. Vos G, le Febre RA, de Graaff RAG, Haasnoot JG, Reedijk J (1983) Unique high-spin-low-spin transition of the central ion in a linear, trinuclear iron(II) triazole compound. J Am Chem Soc 105(6): 1682–1683
38. Kahn O, Martinez CJ (1998) Spin-transition polymers: from molecular materials toward memory devices. Science 279(5347):44–48
39. Peng C, Ayala PY, Schlegel HB, Frisch MJ (1996) Using redundant internal coordinates to optimize equilibrium geometries and transition states. J Comput Chem 17(1):49–56
40. Dennington R II, Keith T, Millam J (2007) GaussView, version 4.1.2. Semichem Inc., Shawnee Mission
41. Frisch MJ, Trucks GW, Schlegel HB, Scuseria GE, Robb MA, Cheeseman JR, Montgomery JA Jr, Vreven T, Kudin KN, Burant JC, Millam JM, Iyengar SS, Tomasi J, Barone V, Mennucci B, Cossi M, Scalmani G, Rega N, Petersson GA, Nakatsuji H, Hada M, Ehara M, Toyota K, Fukuda R, Hasegawa J, Ishida M, Nakajima T, Honda Y, Kitao O, Nakai H, Klene M, Li X, Knox JE, Hratchian HP, Cross JB, Bakken V, Adamo C, Jaramillo J, Gomperts R, Stratmann RE, Yazyev O, Austin AJ, Cammi R, Pomelli C, Ochterski JW, Ayala PY, Morokuma K, Voth GA, Salvador P, Dannenberg JJ, Zakrzewski VG, Dapprich S, Daniels AD, Strain MC, Farkas O, Malick DK, Rabuck AD, Raghavachari K, Foresman JB, Ortiz JV, Cui Q, Baboul AG, Clifford S, Cioslowski J, Stefanov BB, Liu G, Liashenko A, Piskorz P, Komaromi I, Martin RL, Fox DJ, Keith T, Al-Laham MA, Peng CY, Nanayakkara A, Challacombe M, Gill PMW, Johnson B, Chen W, Wong MW, Gonzalez C, Pople JA (2004) Gaussian 03. Revision E.01. Gaussian Inc., Wallingford
42. Becke AD (1993) Density-functional thermochemistry. III. The role of exact exchange. J Chem Phys 98(7):5648–5652
43. Lee C, Yang W, Parr RG (1988) Development of the Colle–Salvetti correlation-energy formula into a functional of the electron density. Phys Rev B 37(2):785–789
44. Krishnan R, Binkley JS, Seeger R, Pople JA (1980) Self-consistent molecular orbital methods. XX. A basis set for correlated wave functions. J Chem Phys 72(1):650–654
45. Frisch MJ, Pople JA, Binkley JS (1984) Self-consistent molecular orbital methods 25. Supplementary functions for Gaussian basis sets. J Chem Phys 80(7):3265–3269
46. Frisch MJ, Head-Gordon M, Pople JA (1990) Semi-direct algorithms for the MP2 energy and gradient. Chem Phys Lett 166(3):281–289
47. Gonzalez C, Schlegel HB (1989) An improved algorithm for reaction path following. J Chem Phys 90(4):2154–2161
48. Gonzalez C, Schlegel HB (1990) Reaction path following in mass-weighted internal coordinates. J Phys Chem 94(14):5523–5527
49. Hobza P, Zahradnik R (1988) Intermolecular interactions between medium-sized systems. Nonempirical and empirical calculations of interaction energies: successes and failures. Chem Rev 88(6): 871–897
50. van Duijneveldt FB, van Duijneveldt-van de Rijdt JGCM, van Lenthe JH (1994) State of the art in counterpoise theory. Chem Rev 94(7):1873–1885
51. Boys SF, Bernardi F (1970) The calculation of small molecular interactions by the differences of separate total energies. Some procedures with reduced errors. Mol Phys 19(4):553–566
52. Miertuš S, Scrocco E, Tomasi J (1981) Electrostatic interaction of a solute with a continuum. A direct utilization of ab initio molecular potentials for the prevision of solvent effects. Chem Phys 55(1):117–129
53. Barone V, Cossi M (1998) Quantum calculation of molecular energies and energy gradients in solution by a conductor solvent model. J Phys Chem A 102(11):1995–2001
54. Cossi M, Rega N, Scalmani G, Barone V (2003) Energies, structures and electronic properties of molecules in solution with the C-PCM solvation model. J Comput Chem 24(6):669–681
55. Tomasi J, Mennucci B, Cammi R (2005) Quantum mechanical continuum solvation models. Chem Rev 105(8):2999–3093
56. Moore WJ (1974) In: Physical chemistry. Longman, London, pp 282–299
57. Atkins PW (1994) In: Physical chemistry. Oxford University Press, Oxford, pp 147–170
58. Özdemir N, Dinçer M, Kahveci B, Ağar E, Şaşmaz S (2003) 4-(*m*-Chlorobenzylamino)-3-phenyl-4,5-dihydro-1*H*-1,2,4-triazol-5-one. Acta Crystallogr E59(8):o1223–o1225
59. Nikolaienko TY, Bulavin LA, Hovorun DM (2011) How flexible are DNA constituents? The quantum-mechanical study. J Biomol Struct Dyn 29(3):563–575
60. Bernstein J, Davis RE, Shimoni L, Chang NL (1995) Patterns in hydrogen bonding: functionality and graph set analysis in crystals. Angew Chem Int Ed Engl 34:1555–1573
61. Iogansen AV (1999) Direct proportionality of the hydrogen bonding energy and the intensification of the stretching ν(XH) vibration in infrared spectra. Spectrochim Acta A 55(7–8):1585–1612